Received: 12 May 2024 | Accepted: 10 June 2025

DOI: 10.1111/2041-210X.70096

Methods in Ecology and Evolution

RESEARCH ARTICLE

Using aerial thermography to map terrestrial thermal environments in unprecedented detail

Karla Alujević[1] | Guillermo Garcia-Costoya[1] | Noa Ratia[1] | Emma Schmitz[1] | Russell S. Godkin[2] | Akhila C. Gopal[1] | Jelena Bujan[3] | Michael L. Logan[1]

[1]Department of Biology and Program in Ecology, Evolution, and Conservation Biology, University of Nevada, Reno, Nevada, USA

[2]Department of Natural Resources & Environmental Science, University of Nevada, Reno, Nevada, USA

[3]Division for Marine and Environmental Research, Ruđer Bošković Institute, Zagreb, Croatia

Correspondence
Karla Alujević
Email: alujevick@gmail.com

Handling Editor: Miguel Acevedo

Abstract

1. The accurate quantification of thermal environments is crucial for predicting the impacts of climate change across ecosystems.
2. Two major obstacles exist in mapping biologically relevant thermal landscapes: (1) overcoming the mismatch between the scale at which environmental data are typically collected and the scale at which a particular organism experiences thermal variation and (2) quantifying thermal landscapes without substantial measurement gaps in time or space.
3. We present a new method that integrates aerial thermography from uncrewed aerial vehicles with field-deployed operative temperature models to generate fine-scale, spatiotemporally complete maps of operative temperature.
4. To ensure the accessibility of our method, we developed an R package, '`throne`', which streamlines the necessary corrections to raw drone data and produces operative thermal landscapes for any day or time during which data loggers were deployed.
5. Our method allows researchers to generate detailed and biologically relevant thermal landscapes for species of interest, which should enhance our understanding of animal thermal ecology and improve our ability to understand the responses of organisms to environmental change.

KEYWORDS
climate change, drone photogrammetry, infrared, operative temperature, remote sensing, thermal imagery

1 | INTRODUCTION

Human activities are rapidly altering the global climate, resulting in significant consequences for organisms across ecosystems (Deutsch et al., 2008; Garcia-Costoya et al., 2023; Sinervo et al., 2010; Thomas et al., 2004). Predicting how organisms will respond to changing thermal environments requires accurate quantification and mapping of current thermal conditions. However, this is hindered by two key challenges: (1) there is a mismatch between the scale at which environmental data are typically collected and the scale at which a

Karla Alujević and Guillermo Garcia-Costoya contributed equally.

particular organism experiences thermal variation, and (2) there can be substantial measurement gaps in time and space. While these are significant challenges for all organisms, they are especially acute for ectotherms that live in the spatiotemporally heterogenous thermal environments that are typical of terrestrial habitats.

Many studies have demonstrated the importance of fine-scale thermal heterogeneity in the ecology and evolution of terrestrial ectotherms (e.g. Alujević et al., 2023; Cox et al., 2018; Cox, Tribble, et al., 2020; Logan et al., 2014, 2015, 2016, 2021; Neel et al., 2021; Potter et al., 2009; Sears & Angilletta, 2015; Williams et al., 2022) despite the fact that numerous researchers continue to incorporate coarse-scale environmental data from sources like WorldClim into their models (Fick & Hijmans, 2017; Karger et al., 2017). Several methods have been developed that partially overcome the challenges of measuring biologically relevant thermal environments. These include the use of biophysical (mathematical) models combined with remote sensing (where operative temperatures are predicted from biophysical theory) or physical models (data loggers) deployed at a field site (where temperatures are measured empirically; Figure S2). These approaches are used to assess 'operative temperature distributions', which can be thought of as null distributions of temperatures that are available to a particular organism in a given space and time and provide information on habitat thermal quality (Bakken, 1992; Dzialowski, 2005). The quantification of operative temperatures has played a pivotal role in the study of animal thermal ecology, physiology, behaviour and evolution (reviewed in Angilletta, 2009), and it has been an irreplaceable tool in understanding ecosystem responses to rapid environmental changes (Gunderson & Leal, 2012; Huey et al., 2012; Logan et al., 2013).

Although the measurement of operative temperatures has been fundamental to our understanding of animal thermal biology and predicting responses to climate change, there are limits to their use and application. Biophysical models require environmental inputs such as air temperature, humidity, wind speed and solar radiation, obtained from weather stations or satellites, which are then integrated with spatial data to simulate organismal heat exchange. Ecophysiological modelling tools (e.g. NicheMapR, Kearney & Porter, 2017; TrenchR, Buckley et al., 2023; microclima, Maclean et al., 2019) have advanced the fields of thermal ecology and global change biology by improving our ability to estimate microclimates. However, these software programs face some limitations in their capacity to translate population-level estimates to the dynamics of individual organisms (Meyer et al., 2023). First, the input of high-quality environmental data is crucial, yet these data are sometimes not available at the temporal and spatial scales at which organisms typically experience their environment. Second, ecophysiological modelling usually requires general assumptions about the ways in which factors like vegetation characteristics, soil properties and topography shape microclimates, and these assumptions can be violated in some situations (Woods et al., 2015). Third, while current software packages can model thermal conditions across a range of microhabitats, most cannot assess the presence, frequency or spatial distribution of these microhabitats in the area of interest without simplifying assumptions, or in areas where high-resolution satellite imagery is not available.

A potentially more tractable approach to quantifying operative thermal environments, particularly for small terrestrial vertebrates, involves the deployment of temperature data loggers that mimic key biophysical properties of the organism of interest (although some challenges remain; Alujević et al., 2024). These loggers are known as 'operative temperature models' (OTMs) and they provide a measurement of the thermal environment at the organism's spatial scale by integrating conductive, convective and radiative heat transfer between the animal and its surroundings (Angilletta, 2009; Bakken, 1976; Bakken et al., 1985). While OTMs can provide near-continuous temporal data (if programmed to record temperatures frequently), they can only offer limited spatial coverage. This spatial limitation is a problem, as it prevents a spatially explicit understanding of thermal heterogeneity at the site, and research had demonstrated that this heterogeneity can significantly influence organism thermoregulation, movement and energetics (Sears et al., 2016; Sears & Angilletta, 2015).

Drones offer a promising solution to the challenge of measuring thermal environments at biologically relevant scales. Their increasing affordability, versatility and ability to access difficult terrain have made them invaluable tools in ecological research (e.g. Aucone et al., 2023; Francis et al., 2022; Saunders et al., 2022). Many commercial drone models now come outfitted with thermal imaging (thermal infrared or 'TIR') cameras, allowing for high-resolution mapping of thermal landscapes via photogrammetry (Thiele et al., 2017; Webster et al., 2018). Yet aerial thermography and OTMs give largely non-overlapping estimates of thermal environments. Although TIR drone-based photogrammetry can produce a thermal landscape that is comprehensive in its spatial coverage, it remains temporally discrete, producing a thermal map for only the time period during which the drone was being flown. Moreover, while OTMs integrate all the relevant forms of heat transfer present in the environment to give estimates of the equilibrium body temperatures that would be achieved by the study organism, the temperature sensors on TIR drones estimate only the heat energy that is emitted from surfaces. Factors such as whether or not the drone was given a warm-up period, the distance between the camera and the surface, the angle of incidence of the sun, ambient temperature, substrate emissivity and wind speed (among others) can influence drone-based TIR estimates (Faye et al., 2016; Jiao et al., 2016; Playà-Montmany & Tattersall, 2021; Yuan & Hua, 2022). In other words, OTMs give temporally complete, but spatially discrete, distributions of operative temperatures, whereas TIR drone photogrammetry gives spatially complete, but temporally discrete distributions of emitted surface temperatures. To achieve the goal of measuring and predicting spatiotemporally complete distributions of operative temperatures, drone-based temperature estimates must be corrected such that they describe operative temperatures and then those temperatures must be extrapolated to days and times when the drone was not flown.

Here, we present a new method that integrates TIR drone photogrammetry with field-deployed OTMs to generate fine-scale, spatiotemporally complete landscapes (maps) of operative temperature

for terrestrial organisms. At its core, our method takes biologically relevant and temporally continuous, but spatially limited, OTM data and extrapolates it to a broad geographic area at high resolution. We developed a new R package called `throne` ('th'ermal d'rone') that streamlines our method and renders it accessible to biologists and conservation managers by requiring minimum user input to produce high-resolution operative temperature maps for any day/time combination during which OTMs were deployed. Finally, we used operative temperature data for the western fence lizard (*Sceloporus occidentalis*) to validate our method at a thermally complex field site in the Great Basin Desert of northern Nevada. Our method for quantifying and predicting terrestrial thermal environments at high spatiotemporal resolution has the potential to increase our understanding of how individuals, and thus populations, will respond to climate warming, habitat conversion and other environmental changes.

2 | MATERIALS AND METHODS

2.1 | `throne` workflow

The general `throne` workflow involves the following steps: (1) Simultaneously collecting operative and emitted surface temperatures (hereafter, 'surface temperatures') using OTMs and a TIR compatible drone, respectively; (2) Integrating these datasets and applying necessary corrections; and (3) Interpolating corrected data across time and space to generate 'predicted' thermal landscapes (Figure 1). The user first assembles a map of surface temperatures of their field site using TIR drone photogrammetry while at the same time collecting operative temperatures using OTMs deployed at microsites that capture local microhabitat diversity. All subsequent steps can be accomplished using our R-package, '`throne`', available on GitHub (https://github.com/ggcostoya/throne). These datasets are then combined such that the relationship between OTM temperatures and drone surface temperatures is assessed and necessary corrections are applied. Finally, OTMs are assigned to tiles (unique latitude and longitude combinations) with similar thermodynamics from the thermal orthomosaic and a high-resolution operative temperature map is then generated for any day and time during which the OTMs were logging. The assembly of thermal landscapes is automated and only requires operative and surface temperature data (with corresponding metadata) and a small number of parameters (e.g. level of smoothing of temporal thermal profiles and desired spatial resolution, date and time for the final thermal landscape; Figure 2) as input. We detail each of the steps below.

2.1.1 | OTM deployment

OTMs should be built to mimic a key set of biophysical properties of the organism of interest (e.g. shape, surface reflectance, conductivity), ensuring that under constant environmental conditions they produce an 'instantaneous' estimate of the equilibrium body temperature that the animal would achieve at the microsites in which the OTMs are deployed. OTMs can be built using different techniques that have varying degrees of practicality and accuracy, although recent advancements in 3D printing can be used to generate highly accurate and cost-effective OTMs for many species (Alujević et al., 2024). For our method to work optimally, OTMs should be deployed strategically across different microhabitats and physiographic features (e.g. substrate types, exposure level, vegetation types, slopes) within the study area to capture a wide range of microclimatic conditions.

2.1.2 | Drone flights

Thermal photogrammetry data are collected using a drone equipped with an IR thermal imaging camera and a GPS unit. A flight plan can be programmed into the drone using photogrammetry software, and this software sometimes comes with the drone when purchased. For our method to be most successful, the following guidelines should be followed: (1) Flights should be conducted under weather conditions that maximize thermal heterogeneity (e.g. sunny weather) as this increases the ability of `throne` to match OTMs with tiles of similar thermodynamics; (2) Flights should be distributed across different days and times to maximize representation of daily temperature fluctuations (modern drones are capable of stable flight in moderate wind and light rain, so data collection can be conducted under a range of conditions), although nighttime flights are likely not necessary because thermal heterogeneity is typically much lower without solar radiation such that flights near dawn and dusk will be sufficient to capture these dynamics; (3) To prevent stitching issues, flights should be conducted over a slightly larger area than the specific area of interest; (4) Flight times should be kept relatively short to ensure that all images are captured during similar site-level thermal conditions and within an ecologically relevant window; (5) The resolution of the mounted thermal imaging camera should be considered when planning flights and choosing flight altitude; (6) The mounted thermal imaging camera should be radiometrically calibrated and produce thermal images in either TIF or R-JPEG file formats; (7) The average emissivity of the site substrate should be assessed to appropriately calibrate the thermal imaging camera; (8) The vertical and horizontal percentage of overlap between photos should be set to a high value (preferably 90% or greater but no less than 70%). Image overlap reduces the measurement error inherent in individual IR images; (9) Ground control points (GCPs) should be deployed as they help to accurately georeference thermal images and minimize processing errors (GCPs should be strategically placed to cover the study site's borders and topographical complexity). After collecting thermal images, photogrammetry software can be used to process images and generate a thermal orthomosaic—a composite snapshot of the thermal landscape. Image processing steps will vary by software type (for more details on this process see the `throne` website: https://ggcostoya.github.io/throne/), although the resulting raster file should be produced in the TIF-file format.

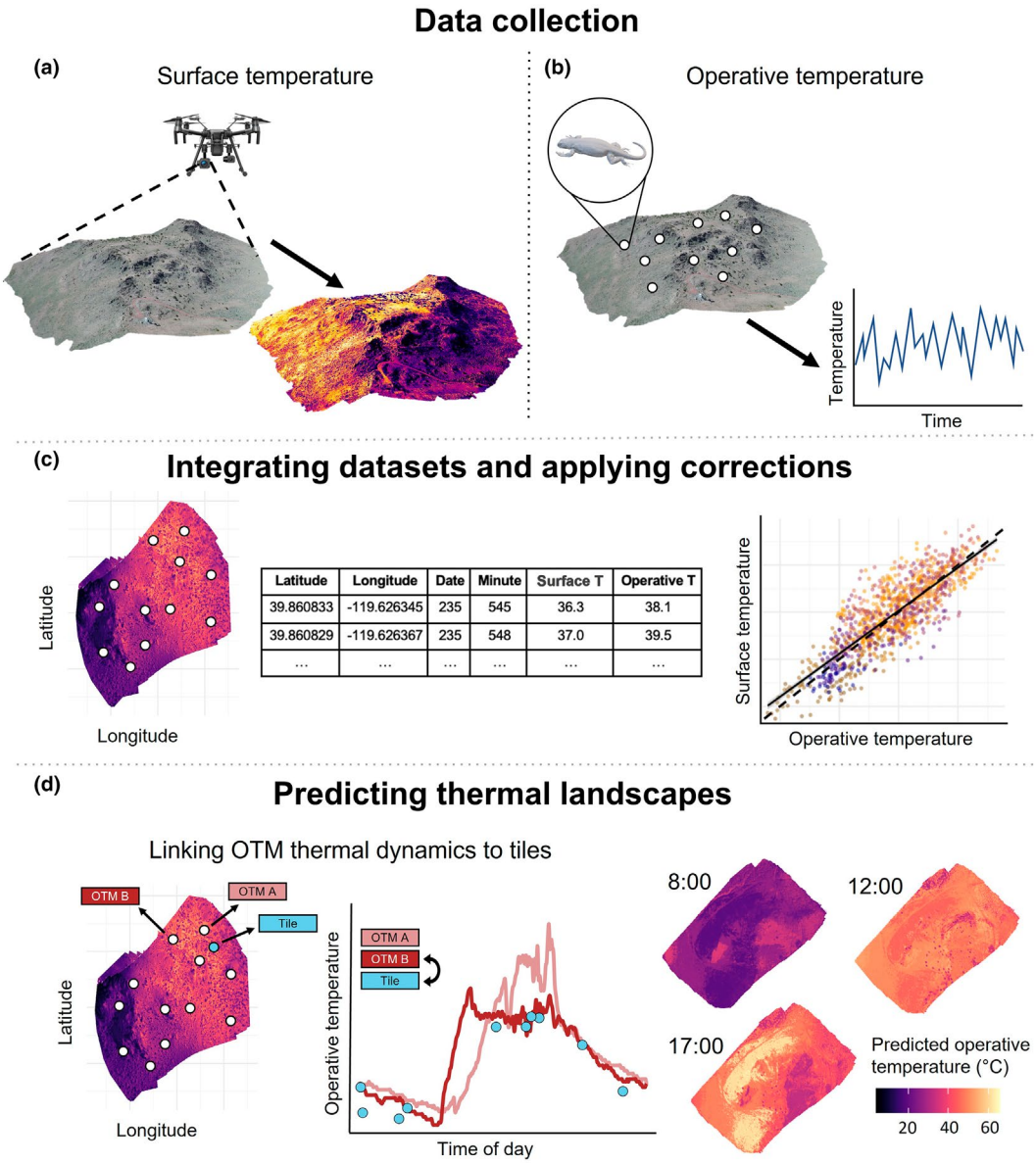

FIGURE 1 General workflow for our method that links thermal infrared (TIR) drone photogrammetry with operative temperature data to produce spatiotemporally complete and biologically relevant thermal landscapes. The practitioner or researcher first assembles a map of surface temperatures of their field site using TIR drone photogrammetry (a) while at the same time collecting operative temperatures using operative temperature models (OTMs) matching the biophysical properties of their study organism and that are deployed across a range of microsites that capture a representative sample of local microhabitat diversity (b). All subsequent steps can be accomplished in our R package, `throne`. (c) These datasets are then combined such that the relationship between OTM temperature and drone-based surface temperature is assessed and necessary corrections are applied. (d) The thermal dynamics of the OTMs are assigned to tiles from the thermal orthomosaic and a high-resolution operative temperature map can then be generated for any day and time during which the OTMs were logging.

2.1.3 | Processing operative temperatures from OTMs

After the OTMs are retrieved from the field and the individual OTM data are downloaded, the OTM data files are then combined into an R data frame, using the `rnp_otms_data` function in `throne`. This function returns a processed data frame with columns for the OTM's identifier, year, day of the year, minute of the day and operative temperature where each row is a unique operative temperature measurement at a given time by a given OTM. Further, `rnp_otms_data` incorporates user-specified metadata in the final output, including the geographic position where the OTM was deployed which, if needed, is projected into Universal Transverse Mercator (UTM) coordinates to ensure compatibility with flights data. Next, the output of the `rnp_otms_data` function is processed using the `gen_otm_spline` function to fit smoothing spline models to each individual OTM for each day during its deployment in the field using the base R native `smooth.spline` function (R Core Team, 2024).

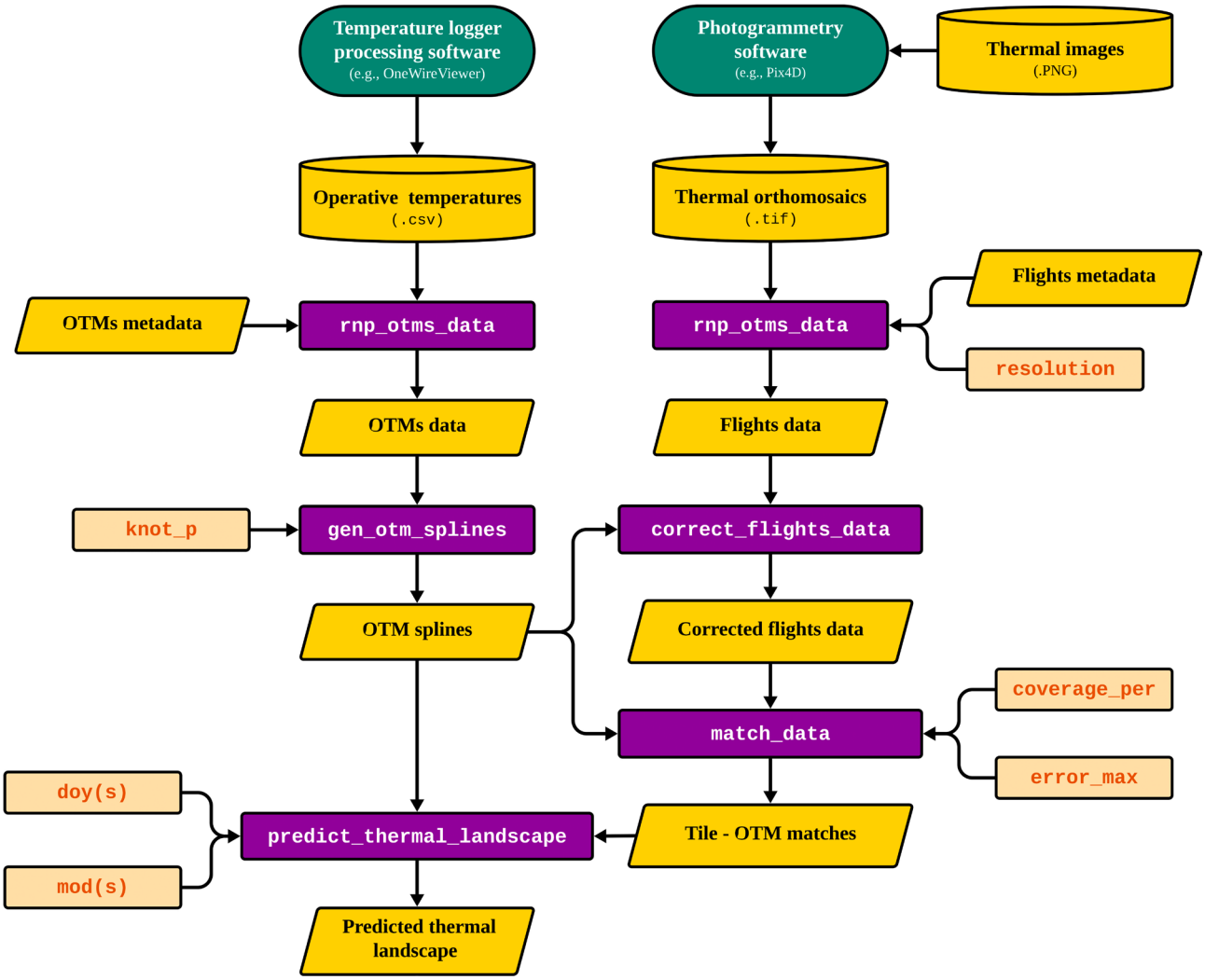

FIGURE 2 The `throne` R-package workflow. Sources of input data are represented by yellow cylinders for databases and yellow tilted squares for single datasets. Green ovals denote software tools external to `throne`. Squares with red font represent user-specified parameter values. Purple rectangles denote embedded functions.

Briefly, these models generate a smoothing function that captures the essential thermodynamics of each OTM throughout a given day. Smoothing minimizes noise from short-term stochastic shifts in operative temperature while capturing fluctuations caused by conditions unique to each day (e.g. sustained changes in cloud cover or wind) that may be ecologically relevant. This approach eliminates the need to collect additional metadata during OTM deployment (e.g. aspect or shade cover) and removes the assumption that within-day thermal fluctuations follow a fixed sinusoidal curve in order to inform the resulting models. Nonetheless, as the level of smoothing may be important in certain systems and may influence the ability of `throne` to match OTMs with orthomosaic tiles, the `gen_otm_splines` function incorporates the parameter `knot_p`. This parameter determines the percentage of observations recorded by an OTM in a given day that are used to determine the number of knots in the spline model (fewer knots equate to more smoothing). The output of the `gen_otm_splines` function inherits all metadata information from the OTM data frame while adding a nested column containing the spline model. The resulting data frame contains as many rows as there were combinations of unique OTM identifier and date as each of these combinations is assigned a fitted spline model.

2.1.4 | Processing surface temperatures from drone flights

Drone flight orthomosaic `.tif` files generated using photogrammetry software are converted into an R data frame using the function `rnp_flights_data`. File `.tif` format is a standard for thermal raster images, containing pixel-wise temperature values generated from radiometrically calibrated sensors (in our case Zenmuse XT2's built-in radiometric calibration; note that file formats like JPEG are not suitable inputs for our approach as they do not preserve the absolute temperature data needed for accurate thermal predictions). The rnp_flights_data function first reads the `.tif` file as a `spatRaster` within the R environment using functionality from the package

terra (Hijmans, 2020). Second, the function summarizes the data to the desired spatial resolution via the argument resolution. The resolution argument determines the area covered (in m^2) by each of the orthomosaic tiles of the final output and it can be set to any value ≥0.5 m^2. Lastly, the function adds user-specified metadata to the processed flight dataset including values for year, day-of-year and minute of the day at which the flight started and ended. The final output is a data frame with columns for geographic position indicated by an 'x' and 'y' coordinate within the UTM zone where the flight took place, time (year, day-of-year, minute of the day at which the flight started and ended) and surface temperature. In this data frame, each row corresponds to the surface temperature in a given tile (unique x-y combination) of an individual flight.

2.1.5 | Integrating OTM and drone data

Due to the fundamental differences in the physical properties of surface (IR-based) and operative (OTM-based) temperature measurements, the data frames representing thermal maps obtained via the rnp_flights_data function need to be corrected such that they represent operative temperatures. To achieve this, throne includes the correct_flights_data function. First, the function identifies all tiles within the study area that contained OTMs, and 1) gathers all the temperature measurements of those tiles collected across multiple flights, and 2) estimates the temperature experienced by all OTMs at the exact set of dates and times when each of the flights took place using the spline models obtained via the gen_otm_splines function. Second, the function estimates the average bias between surface and operative temperature measurements for each flight (Figures S5 and S6) and subtracts this bias from all surface temperature measurements. This first correction step is needed because the magnitude of the difference between the OTM and surface temperatures can vary systematically between days and by time-of-day due to the difference in the way these different measurements respond to ambient temperature, solar angle, overall light availability, etc. However, the function offers users the ability to choose which metric they prefer as the basis for surface temperature correction (average, median or mode), or the option to skip the correction step entirely. Lastly, the function inspects the relationship between surface temperature (which the user may or may not have chosen to correct for date and time-of-day) and operative temperature by fitting a simple linear regression between these variables. If temperature measurements collected by the drone were perfectly unbiased estimates of operative temperature, the relationship between these two variables would be 1:1 (intercept = 0 and slope = 1). To achieve this 1:1 relationship, the function applies a second correction following the equation:

$$OT = \frac{ST - \alpha}{\beta},$$

where ST and OT are surface and operative temperatures, respectively, and α and β are the intercept and slope of the relationship between ST and OT across all tiles where OTMs were deployed. To give further control over how this correction step is performed, correct_flights_data also offers users the possibility of applying this step while accounting for day- and time-specific relationships. In this case, the correction is applied via the equation:

$$OT = \frac{ST - \alpha - \beta_2 DOY - \beta_3 MOD}{\beta_1},$$

where β_1 is the effect of OT on ST (same parameter as β in the previous equation) while β_2 and β_3 are the effects of day of the year (DOY) and median minute of the day when the flight took place (MOD), respectively.

2.1.6 | Predicting thermal landscapes

The last step of the throne workflow is generating a thermal landscape for a specific time of interest. This is achieved via the match_data and predict_thermal_landscape functions. First, the match_data function matches each tile in the thermal orthomosaic with an OTM based on the similarity in their thermodynamics. For each tile, the function calculates the average absolute difference between the temperatures recorded in that tile across multiple flights (previously corrected through the correct_flights_data function), and the temperatures extracted from all OTM splines at the same time the flight took place. OTMs do not need to have logged temperatures at the exact time the flight took place as the operative temperatures are predicted from the date-specific OTM spline function (gen_otm_splines). To assign a match to a tile, the match_data function chooses the OTM that minimizes the absolute difference between temperature measurements. For some tiles, it is possible that their thermodynamics are still notably different from those of the OTM that best describes it among the OTMs deployed (i.e. that the average absolute error is substantially large). To account for that, users can specify the maximum error they are willing to tolerate for a tile's thermal profile to be included in their final output by setting the error_max parameter (if the minimum error is larger than error_max, the pixel is not assigned an OTM). If it is not specified, error_max will default to 100, a sufficiently large number to permit any match, which in turn allows users to explore the quality of their matching (Figure S13) and perform any diagnostics or quality control efforts they see fit. The resulting output of the match_data function is a data frame where each tile is associated with a character indicating the identifier of the OTM that best describes its thermodynamics. Finally, the predict_thermal_landscape function takes the output of the data frame obtained through match_data and calculates the predicted operative temperature in each tile at a user-specified date and time using the OTM and date-specific cubic spline models fitted through the gen_otm_splines function. Through this approach, users can predict a thermal landscape for any date and time (minute of the day) within the general period when OTMs were logging (i.e. for all days in which there are fitted spline models). The final output is a data frame with six columns, indicating

the year, day of year, minute of the day, x and y UTM coordinates and predicted operative temperature for that specific tile.

2.2 | Validation

To validate our approach to mapping operative thermal environments, we tested (1) whether the predicted thermal landscape outputs by `throne` are accurate for microsites where OTMs were not deployed and (2) the sensitivity of the method to different user choices (e.g. number of drone flights, number of OTMs, level of spline smoothing). To accomplish this, we conducted two validations where we compared the operative temperatures predicted by `throne` with those recorded by OTMs that had been withheld from the workflow. With our validations we demonstrate how changing the number of flights conducted, OTMs deployed, and spatial and temporal scale affect the accuracy and utility of our method. Here, we present the methods and results for validation 1, which was conducted over a 76-day period and for a ~33,000 m^2 study area, with 10 flights and 73 OTMs. Validation 2 took place over 3 days within a smaller area (600 m^2) but involved a higher frequency of flights (34), and we present detailed methods and results for this validation in Supporting Information. Our methodology was approved by the University of Nevada, Reno Institutional Animal Care and Use Committee (protocol 21-02-1129) and the Nevada Department of Wildlife (permit number 41066). For each validation, we executed the complete `throne` pipeline with different combinations of parameters (subset of flights, subset of OTMs and `knot_p` values). Below, we detail how we collected data to conduct validation 1 in the context of our study system (for the list of best practices and recommendations see Box S1 in Supporting Information and `throne` website: https://ggcostoya.github.io/throne/).

2.2.1 | OTM deployment

We deployed 73 OTMs on April 15th, 2023, across a 33,000 m^2 area southwest of Pyramid Lake in Washoe County, Nevada, USA (39.865 N, 119.624 W). This site is in the Great Basin Desert and is characterized by a thermally complex array of ridges and rocky outcrops (Figure S1). The vegetation community is dominated by big sagebrush (*Artemisia tridentata*), saltbush (*Atriplex gardneri*), pinyon pine (*Pinus monophylla*) and juniper (*Juniperus osteosperma*). We 3D printed our OTMs using acrylonitrile butadiene styrene (ABS) for studies of the thermal ecology of the western fence lizard (*Sceloporus occidentalis*; Figure S2), a species that is abundant at our field site, and for which we previously validated 3D printed OTMs against live lizards in the field (Alujević et al., 2024; for general recommendations on building OTMs and ensuring that OTM mimics the species of interest also see Dzialowski, 2005). We centrally suspended a temperature logger (iButton, accuracy of 0.5°C, Embedded Data Systems, Lawrenceburg, KY) inside each model and set each logger to record temperature every 50 min (~29 measurements/day). We obtained operative temperature measurements from the loggers for 119 days from April 16 to August 19, excluding June 11, 12 and 27–29 (these were days when we had to retrieve OTMs to download data due to the limited storage capacity of iButtons). This time period and geographic area encompassed significant seasonal and spatial thermal variation (Figure S3). We distributed OTMs across microhabitats that are typical of this site (for detailed descriptions of these microhabitats see Table S1) and at different orientations to capture a range of ecologically relevant microsites based on our previous experience working with this species in this environment. For each OTM, we recorded its position in a World Geodetic System projection (WGS; i.e. latitude and longitude) using a high accuracy (<1 m^2 resolution) Trimble Geo7x handheld GPS unit (Trimble, Westminster, CO).

2.2.2 | Drone flights

We created a flight mission using DJI Pilot software (v 1.1.5; DJI, Shenzhen, China) that was larger (52,000 m^2) than the area covered by our OTMs to ensure that the central area of interest was fully covered by the drone transects. We placed four GCPs within the borders of the OTM deployment area, covering approximately the highest, middle and lowest elevation (Agüera-Vega et al., 2017). We recorded each GCP's position in WGS projection using the same Trimble Geo7x handheld GPS unit. The flight altitude was set at 100 m above ground level (AGL), resulting in a ground sample distance (GSD) of 13.08 cm/pixel. The mission flight speed was 5.3 m/s, with a 70% side to 80% frontal image overlap ratio. Thermal and RGB images were collected simultaneously in-flight using a FLIR Zenmuse XT2 infrared camera (focal length = 13 mm, TIR resolution = 640 × 512, spectral range = 7.5–13.5 μm, accuracy = <0.05°C @ f/1.0, file format = TIFF/R-JPEG/JPEG and emissivity = 1.0) mounted on a DJI Matrice 200 Series V2 quadcopter. Thermal and RGB data were captured in R-JPEG and JPEG formats, respectively. We conducted 10 mission flights between 8:30 AM and 7:45 PM in the period between May 15 and July 29, 2023 (Table S2). General conditions before each flight were recorded using a Kestrel 3000 weather meter. The average wind speed (±SD) across all flights was 3.9 ± 4.3 m/s and the average air temperature was 23.5 ± 11.5°C. We flew 8 of these missions under sunny and/or clear conditions whereas two occurred during light cloud cover, conditions that are representative of the typical weather experienced at our field site during summer months.

We processed all drone imagery using the Thermal Camera processing template in Pix4Dmapper (version 4.8.4; Pix4D; Prilly, Switzerland). We included both thermal and RGB images in the template with the following changes to the default settings for thermal image processing: The Point Cloud Point Density was set to 'high' and the orthomosaic was generated as a GeoTIFF with 'merge tiles' enabled. We georeferenced all images using GCPs to ensure maximum accuracy. We successfully generated 34 orthomosaic raster images and created a `.tif` file for each of the processed flights, with

a Root Mean Square error (the difference between the initial and computed positions of the GCPs) of 0.0475 ± 0.0063 m (mean ± SD) and an average orthomosaic GSD of 4.44 ± 0.474 cm/pixel. To test for the effect that using GCPs had on the accuracy of the final thermal landscape output of `throne`, we generated an alternative set of orthomosaic raster images during which we skipped the georeferencing step.

2.2.3 | Data processing

After the iButtons were retrieved from the field, we downloaded the data using OneWireViewer software (Analog Devices, Inc., Wilmington, MA) and ran the data through the `throne` workflow. We used the `rnp_otms_data` function to process all raw OTM data into a single data frame, which we later used to fit OTM and date-specific cubic splines using the `gen_otm_splines` functions. To test how the choice of smoothing parameter (`knot_p`) affected the accuracy of our predictions, we fitted cubic splines with three different knot_p values (see below). Flight-specific orthomosaic `.tif` files (both GCP-referenced and not) were imported into R and converted into data frames using the function `rnp_flights_data`. For the latter function, we set the `resolution` to 1, resulting in a spatial resolution of 1 m^2 for the thermal landscape, an area that is ecologically relevant to western fence lizards based on their body size and home range as determined by our research group previously (unpublished data) and by studies in other populations in the western USA (Davis & Ford, 1983; Sheldahl & Martins, 2000).

2.2.4 | Predicting thermal landscapes

To validate that the final thermal landscapes produced by our method can accurately estimate operative temperature in areas of field sites where OTMs were not deployed (Garcia-Costoya, unpublished data), we generated a predicted thermal landscape from a subset of our deployed OTMs and then compared predicted operative temperatures to actual (observed) operative temperatures for the tiles that contained the remaining OTMs. We examined how three parameters influenced `throne`'s predictive accuracy: number of drone flights, number of OTMs deployed and the `knot_p` smoothing parameter. We assessed the number of flights and OTMs required to produce accurate thermal landscapes as these factors are likely the most important from a logistical and budgetary standpoint and therefore may reduce the usefulness of our method for some practitioners. We were also interested in examining the effect of `knot_p` as this parameter will determine the sensitivity of our method to short-term fluctuations and thus our ability to accurately predict highly temporally variable landscapes. To examine how variation in these parameters affects the accuracy of the final predicted thermal landscape, we ran the entire `throne` workflow a total of 52 times, predicting operative temperature landscapes using different numbers of drone flights (3, 5 or 10), OTMs deployed (10, 30 or 70) and knots for the spline models (0.25, 0.5 or 1 which are equivalent to 0.3, 0.6 and 1.2 knots/h). The individual drone flights and OTMs used to evaluate each combination of parameters were randomly sampled and we replicated the test 10 times per combination of parameters. In the case of the drone flights, they were separated between being conducted in the morning (before 10:00), middle of the day (between 10:00 and 16:00) and evening (after 16:00) and sampled evenly across these three categories. For each combination of parameters, we calculated the differences between the actual OTM measurements and the predicted operative temperatures from the thermal landscapes for 100 random combinations of dates and times for the period during which OTMs were deployed.

3 | RESULTS

3.1 | Integration of OTM and drone data

Raw surface temperatures obtained from the drone (whether or not images were georeferenced using GCPs) were positively and significantly correlated with operative temperatures obtained from OTMs ($p < 0.001$ for both cases). However, the relationship between surface and operative temperatures obtained from non-georeferenced images was noticeably worse (intercept = −0.28, slope = 0.9, $R^2 = 0.562$, df = 341) than that obtained from georeferenced images (intercept = −0.14, slope = 0.87, $R^2 = 0.62$, df = 351; Figure S4). The correction process implemented via the `correct_flights_data` function (including correcting for day and time-of-day bias; Figure S5) resulted in further improvement of the fit between OTM and surface temperatures while minimally impacting the form of the relationship (intercept = 0, slope = 1, $R^2 = 0.61$, df = 351; Figure S4).

When using all flights and OTMs, and a `knot_p` value of 0.5 (equivalent to 0.6 knot/h at a sampling rate of 1.2 OTM measurements per hour) to predict the full thermal landscape, half of the thermal variability across our field site was explained by as few as five OTMs, with 22 OTMs explaining 90% of the overall thermal variability (Figure 3). OTMs that were deployed at similar orientations (e.g. those deployed on surfaces that faced a particular cardinal direction) tended to be matched with spatially aggregated clusters of tiles which were in the parts of the habitat that faced those directions (Figure 3). We show predicted thermal landscapes generated for our study site in Figure S7.

3.2 | Predictive accuracy

When we used 70 OTMs, 10 flights and set `knot_p` to 1 (i.e. 1 knot/h) to generate the predicted thermal landscape, the mean predictive error (the difference between predicted and observed operative temperature) was 0.187 ± 0.594°C (mean ± SD). When only 10 OTMs and 3 flights were used to generate the predicted thermal landscape (also with `knot_p` set to 1), the mean predictive error was −0.388 ± 0.411°C. In all cases, the 95% confidence interval around the mean predictive

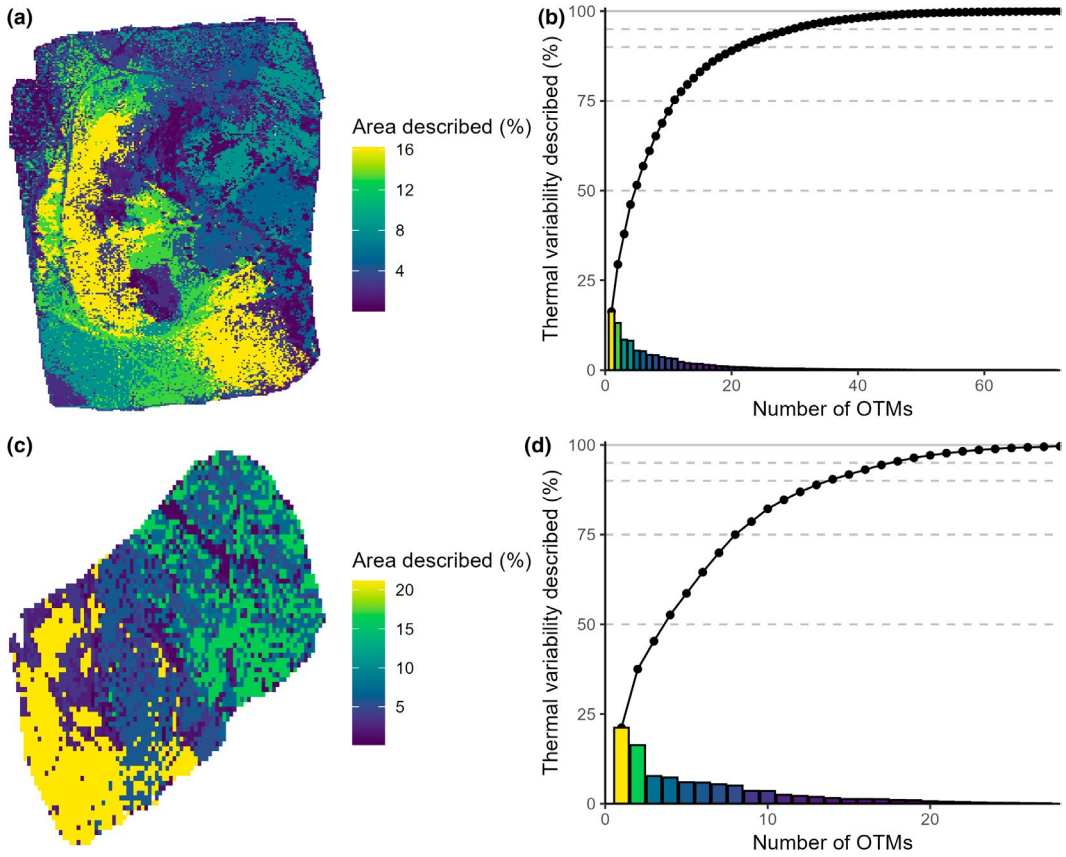

FIGURE 3 A small number of operative temperature models (OTMs) described most of the thermal variation within our field site, whether we used our method to predict operative temperatures over a longer span of time (76 days) and a larger geographic area (33,000 m^2; validation 1; a, b) or over a shorter span of time (3 days) and a smaller geographic area (600 m^2; validation 2; c, d). The solid lines in the panels on the right show the cumulative thermal variation explained by a given number of OTMs. Twenty-two OTMs described more than 90% of the thermal variation for the larger area (b), whereas 15 OTMs described the same amount of thermal variation for the smaller area (d).

Validation 1		knot_p (knot/h)		
N flight	*N* OTM	0.25 (~0.3)	0.5 (~0.6)	1 (~1.2)
3	10	0.52 ± 0.455	0.033 ± 0.578	−0.388 ± 0.411
	30	0.419 ± 0.421	0.398 ± 0.261	−0.097 ± 0.312
	70	0.474 ± 0.262	0.207 ± 0.263	0.792 ± 0.388
5	10	0.725 ± 0.95	0.392 ± 0.261	−0.666 ± 0.292
	30	0.827 ± 0.69	0.127 ± 0.436	−0.158 ± 0.263
	70	0.909 ± 0.824	−0.159 ± 0.383	−0.259 ± 0.25
10	10	0.582 ± 0.745	0.382 ± 0.479	−0.003 ± 0.439
	30	0.472 ± 0.417	−0.318 ± 0.385	0.452 ± 0.716
	70	0.704 ± 1.243	0.679 ± 1.064	0.187 ± 0.594

TABLE 1 Mean predictive error (±SD) for validation 1, presented as the relative difference between the observed (from operative temperature models [OTMs]) and predicted (from the final thermal landscape output by `throne`) temperatures across different combinations of number of drone flights, number of OTMs and knot_p values (magnitude of smoothing of raw OTM data; knots per hours are given in the brackets) used to generate the final thermal landscape. All comparisons were done for data collected during daytime hours (7 AM to 7 PM).

error overlapped with zero. The accuracy of our method did not differ between the two validations; a full list of mean predictive errors (±SD) for both validations and all combinations of flight number, OTM number and number of knots per hour are presented in Table 1 and Tables S3–S5 (reported as both relative and absolute predictive error). Frequency distributions of predictive errors across different combinations of parameters are shown in Figures S8–S12.

4 | DISCUSSION

The traditional approaches to measuring terrestrial thermal environments and predicting how they will change in the future face challenges due to limited availability of high-resolution environmental data. Our method, which integrates drone infrared imaging with in situ OTM measurements, is a tractable approach to measuring

terrestrial thermal environments at high spatiotemporal resolution. Importantly, our method generates thermal maps that are biologically relevant to the study species, at least to the extent that OTMs are properly designed and calibrated for the organism of interest. We have made our method accessible to researchers and practitioners by developing an R package, `throne`, which streamlines the necessary corrections to raw drone data and produces operative thermal landscapes with minimal input and technical expertise required by the user. This approach should enhance the accuracy and accessibility of detailed and biologically relevant thermal landscapes for species around the globe and improve the quality of the baseline data that are required for understanding the responses of organisms to environmental change.

Our method works by linking temporally continuous (but spatially discrete) OTM thermal profiles to spatially continuous (but temporally discrete) thermal orthomosaics generated from drone photogrammetry to generate spatiotemporally comprehensive operative temperature maps (i.e. thermal landscapes). We confirmed that our approach can produce accurate thermal landscapes by comparing the predicted temperatures from the `throne` output to real operative temperatures measured with OTMs that we deployed in the field. Our method produced estimates of operative thermal landscapes that can be considered accurate based on the thermal ecology of Sceloporine lizards (Andrews et al., 1999; Lemos-Espinal et al., 2001; Plasman et al., 2024). Indeed, despite the temporal or spatial scale over which we made predictions, the average predictive error of final daytime thermal landscapes was <0.5°C, and 95% of the tile values within the landscapes were within 2°C of the true value. This accuracy further increases when nighttime temperatures are included (as there is much less thermal heterogeneity at night). Nonetheless, the accuracy and thus utility of our method depends on the optimization of several factors.

First, successful implementation of this method depends on obtaining accurate in situ operative temperature data using field-deployed data loggers (OTMs). In the field of thermal ecology, OTMs are designed in inconsistent ways and often are not properly calibrated (Dzialowski, 2005). However, recent advances in 3D printing provide opportunities to build affordable and accurate OTMs for a wide range of species (Alujević et al., 2024). Since our method involves correlating the thermal profiles of OTMs with tiles in the drone-acquired orthomosaics, it is crucial to deploy OTMs across diverse microhabitats, encompassing various substrates, vegetation types and topographical features. This ensures a comprehensive range of options for linking OTM thermal profiles to tiles. The selection of microhabitats for OTM deployment should be informed by the ecology of the species under study. In our investigation, we strategically deployed OTMs with the goal of comprehensively sampling the microhabitats available to our study species. This allowed us to test the sensitivity of our method to OTM coverage in the thermally heterogeneous environment of the Great Basin Desert. Irrespective of whether we were predicting thermal landscapes across smaller or larger geographic areas, or over shorter or longer time periods, fewer OTMs than we expected were required to describe the thermal dynamics of the site. For an area of 33,000 m^2 and over a 76-day period (validation 1), we found that only five OTMs were required to accurately describe half of the thermal variation at our site, while only 22 OTMs were required to accurately describe 90% of the thermal variation. This promising result suggests that, as long as OTMs are deployed strategically to capture key microhabitat and physiographic features of the site, researchers may not need to deploy large numbers of OTMs for optimal implementation of our method, especially in environments that are less thermally heterogeneous than a rocky desert. Regardless, decisions on how many OTMs to deploy at a given site will be system specific.

A second consideration is the appropriate smoothing factor (i.e. the number of knots per hour; Figure S14) to generate daily thermal profiles for each OTM. This decision depends on two factors: the frequency at which OTMs recorded operative temperatures and the biophysical ecology of the study organism. While it is essential to capture accurate thermal profiles of specific microsites, excessive precision in these profiles will introduce noise that is irrelevant to the study organism and might negatively impact the quality of the match between the thermodynamics of OTMs and tiles from the drone data. What counts as 'excessive precision' will be system-dependent. For example, in an environment where abrupt changes in weather (e.g. gusts of wind, brief cloud cover, etc.) result in rapid and reversible shifts in temperature that are unlikely to influence the behaviour of the organism (because the particular organism has relatively high body mass and therefore relatively high thermal inertia, for example), smoothing improves the quality of the final estimated thermal landscape. This was generally the case for our focal population of the western fence lizard (average adult mass >20 g), and we therefore opted to use 4 knots/h, which smoothed OTM measurements at 15-min intervals. However, for smaller-bodied organisms that are more susceptible to short-term changes in abiotic conditions (e.g. lizards or insects under 5 g in mass), one might increase the number of knots in order to capture shorter-term thermal fluctuations in the environment.

A third factor that we thought would influence the quality of the thermal landscapes produced by `throne` was the number of drone missions flown over the field site. Although we had assumed that a larger number of flights would be advantageous as it would provide more time points to correlate OTM thermal profiles with tile dynamics, our results show that a relatively small number of flights is probably sufficient for most applications. Regardless of whether thermal landscapes were generated using 3 randomly selected flights or 34, and whether operative temperature predictions were made for longer or shorter time periods, or over larger or smaller geographic areas, the accuracy of `throne`'s output was similar (Table 1). This result is likely robust as we tested our method in the highly heterogeneous environment of a high-elevation, temperate desert. This is a notable advantage of `throne`, as the researcher or practitioner will only have to fly their drone a moderate number of times to accurately capture the temporal thermal dynamics of their field site. This should increase the number of missions or size of the field site that

can be measured under the same drone battery power, which can be an important rate-limiting factor in drone-based studies.

Finally, it is important to consider the spatial resolution of drone-based surface temperatures that is necessary to capture thermal variation at a scale that is relevant to the study organism. There are two parameters to consider: (1) the resolution that can be attained by the specific brand and model of TIR camera being used and (2) the resolution of the resulting thermal landscapes that are produced with `throne` (Figure S15). TIR cameras typically produce images with a lower digital resolution than standard cameras (the Zenmuse XT2 thermal camera that we used has a resolution of 640 × 512 pixels). Flight altitude is also important to consider as it affects both the spatial resolution captured by the thermal camera (the size of the pixel on the ground represented by the GSD) and the amount of atmospheric interference between the ground and the sensor (Playà-Montmany & Tattersall, 2021). Users should adjust the flight altitude to generate thermal orthomosaics with a GSD that will ultimately generate a map with a resolution relevant to their focal organism. For example, at a flight altitude of 40 m, the centre distance between two adjacent pixels in our thermal photos was 5.23 cm (each pixel was 0.027 m^2 in area). A flight conducted at lower altitude could be needed for small organisms such as insects. However, using drone temperature data with an extremely low GSD might introduce noise that reduces the predictive capacity of the model. The spatial resolution of the final thermal landscape can also be modulated in `throne` with the argument `resolution` in the `rnp_flights_data` function. Although it would seem logical to always maximize the resolution such that 1 tile represents the smallest possible area (0.5 m^2), increased spatial resolution requires greater computing power and time (especially during the tile-to-OTM matching step), which may not be available to some users. Despite these considerations, our approach will allow researchers to generate thermal landscapes for their study organisms with substantially higher resolution than those commonly used in climate models (e.g. the WorldClim 2 dataset; https://www.worldclim.org/; Fick & Hijmans, 2017).

Major benefits of the `throne` package are that the expertise required to model thermal landscapes at nearly unprecedented levels of spatiotemporal detail is relatively low, the equipment required is relatively affordable, and the thermal landscape model produced is based on real operative temperatures collected at the specific site of interest. While ecophysiological models are invaluable for simulating body temperatures at broader geographic scales, our approach allows for spatially explicit, high-resolution mapping of operative temperatures that are relevant to individual organisms without the need for assumptions or separate measurements of microhabitat frequencies and distributions. Further, our method is applicable to a wide range of open and semi-open environments that occur over broad swaths of the planet.

We have designed `throne` to be user-friendly in that it requires minimal analytical expertise; users can simply input their raw data and a few boundary parameters, and `throne` will generate predicted thermal landscapes for any day/time combination during which OTMs were logging temperatures in the field. To generate the input data, some training and expertise is required, but we do not think this will be insurmountable for most researchers. Thermal biologists have been building and deploying OTMs for decades (Angilletta, 2009; Bakken, 1992; Dzialowski, 2005), and modern commercially available drones with TIR cameras are both relatively affordable and easy to operate. Drones equipped with thermal sensors are rapidly becoming more affordable; the model used in this study was priced at ~USD 8000 in 2019 and the thermal sensor had to be purchased separately (~USD 13,000). Only a few years later, drones with similar capabilities and built-in thermal sensors have become much smaller and more portable, with options like the DJI Mavic 3 Thermal now available for as little as USD 5000. Although the photogrammetry software used in this study (Pix4D) requires a licence, there are several equivalent products that are now available for free (e.g. OpenDroneMap online software: https://www.opendronemap.org/). Despite this, some researchers (especially some of those in developing nations) may find our method too expensive or impractical, perhaps until drone and sensor prices decline further. Regardless, we see the accessibility of our method as a significant advance in the field because it will enable many researchers, practitioners or conservation managers to precisely characterize the thermal environment of interest in a way that is both spatiotemporally comprehensive and relevant to the biology of their study organism.

Although our approach offers numerous benefits, there will be contexts in which it may not be the most appropriate method for quantifying operative thermal landscapes. First, it relies on in situ operative temperature measurements to convert drone-based surface temperatures to temperatures that are biologically appropriate for the study species. This means that `throne` can only be applied during the time period that operative temperatures are being logged by field-deployed OTMs. In this study, we used OTMs that had Thermocron iButton temperature loggers suspended inside. However, even high-capacity iButtons can only record a few thousand temperature measurements. To create thermal landscapes for many months or the entire year, we would have had to retrieve the temperature loggers, download the data and redeploy them several times. This process might not be feasible in other systems where accessing the OTMs is challenging or data storage capacity is limited. Finally, our approach is ideal for environments that are at least moderately open (e.g. deserts, grasslands, open woodlands, etc.). This is because drone thermal imagery can, by its nature, only capture temperatures of surfaces below the flight path. In habitats with fully enclosed canopies, this approach would not be suitable as the drone sensors would be unlikely to penetrate to the understory except in cases where there were canopy gaps (but see alternative approach in Higgins et al., 2024). Nonetheless, our drone-based approach to mapping thermal environments is probably unnecessary in these types of highly buffered, thermally homogeneous environments as the deployment of a small number of temperature loggers usually captures the operative thermal dynamics in these habitats (Cox, Alexander, et al., 2020; Nicholson et al., 2022; Williams et al., 2022).

Furthermore, in addition to its primary application for high-resolution operative thermal mapping, `throne` could also be implemented using `.tif` format datasets from satellite-derived surface temperature products, such as those from VIIRS, Copernicus or MODIS, which offer coarser spatial resolution but can cover broader geographic regions. While this may not capture fine-scale thermal variability, it could still provide valuable insights for large-area studies when combined with ground-based OTMs.

The accurate mapping of terrestrial thermal environments has direct implications for predicting organismal responses to rapid environmental change. Inaccurate or low-resolution estimates of operative temperature can reduce our ability to quantify constraints on thermoregulatory capacity, which generates inaccuracies and biases in our predictions for how organisms might respond to changing environments. Our drone-based framework for quantifying operative thermal environments offers a straightforward approach that produces accurate and precise spatiotemporal operative temperature distributions. The broad adoption of this approach should deepen our understanding of how organisms interact with their environments, how they have adapted to these environments in the past, and how climate change is likely to impact ecosystems in the future.

AUTHOR CONTRIBUTIONS

Karla Alujević, Guillermo Garcia-Costoya, Jelena Bujan and Michael L. Logan conceived the ideas and designed methodology. Karla Alujević, Guillermo Garcia-Costoya, Noa Ratia and Akhila C. Gopal collected the data. Karla Alujević, Guillermo Garcia-Costoya, Noa Ratia, Emma Schmitz and Russell S. Godkin analysed the data. Guillermo Garcia-Costoya led the development of the R package. Karla Alujević and Guillermo Garcia-Costoya led the writing of the manuscript. All authors contributed critically to the drafts and gave final approval for publication.

ACKNOWLEDGEMENTS

We would like to thank Matthew Gifford, Christopher Halsch, Matt Forister, Lee Dyer, Madeleine Lohman and Julia Brockman for their helpful feedback while developing this method and, especially, Matthieu Bruneaux for the thorough review and feedback provided on the R package.

FUNDING INFORMATION

This study was funded by the startup funding awarded to Michael L. Logan at the University of Nevada, Reno, and was not supported by any other grants or funding bodies.

CONFLICT OF INTEREST STATEMENT

The authors declare no competing interests.

PEER REVIEW

The peer review history for this article is available at https://www.webofscience.com/api/gateway/wos/peer-review/10.1111/2041-210X.70096.

DATA AVAILABILITY STATEMENT

Data available via https://doi.org/10.5281/zenodo.15675999 (Garcia-Costoya, 2025).

ORCID

Karla Alujević https://orcid.org/0000-0002-0321-2549
Jelena Bujan https://orcid.org/0000-0002-7938-0266
Michael L. Logan https://orcid.org/0000-0003-2242-1810

REFERENCES

Agüera-Vega, F., Carvajal-Ramírez, F., & Martínez-Carricondo, P. (2017). Assessment of photogrammetric mapping accuracy based on variation ground control points number using unmanned aerial vehicle. *Measurement*, *98*, 221–227. https://doi.org/10.1016/j.measurement.2016.12.002

Alujević, K., Bakewell, L., Clifton, I. T., Cox, C. L., Frishkoff, L. O., Gangloff, E. J., Garcia-Costoya, G., Gifford, M. E., Glenwinkel, M., Gulati, S. A. K., Head, A., Miles, M., Pettit, C., Watson, C. M., Wuthrich, K. L., & Logan, M. L. (2024). 3D printed models are an accurate, cost-effective, and reproducible tool for quantifying terrestrial thermal environments. *Journal of Thermal Biology*, *119*, 103762. https://doi.org/10.1016/j.jtherbio.2023.103762

Alujević, K., Streicher, J. W., Garcia, R. A., Riesgo, A., Taboada, S., Logan, M. L., & Clusella-Trullas, S. (2023). Mismatches between phenotype and environment shape fitness at hyperlocal scales. *Proceedings of the Royal Society B: Biological Sciences*, *290*(2000), 20230865. https://doi.org/10.1098/rspb.2023.0865

Andrews, R. M., Méndez-de la Cruz, F. R., Cruz, M. V. S., & Rodríguez-Romero, F. (1999). Field and selected body temperatures of the lizards *Sceloporus aeneus* and *Sceloporus bicanthalis*. *Journal of Herpetology*, *33*, 93–100.

Angilletta, M. J. (2009). *Thermal adaptation: A theoretical and empirical synthesis*. Oxford Univ. Press.

Aucone, E., Kirchgeorg, S., Valentini, A., Pellissier, L., Deiner, K., & Mintchev, S. (2023). Drone-assisted collection of environmental DNA from tree branches for biodiversity monitoring. *Science Robotics*, *8*(74), eadd5762. https://doi.org/10.1126/scirobotics.add5762

Bakken, G. S. (1976). A heat transfer analysis of animals: Unifying concepts and the application of metabolism chamber data to field ecology. *Journal of Theoretical Biology*, *60*(2), 337–384. https://doi.org/10.1016/0022-5193(76)90063-1

Bakken, G. S. (1992). Measurement and application of operative and standard operative temperatures in ecology. *American Zoologist*, *32*(2), 194–216. https://doi.org/10.1093/icb/32.2.194

Bakken, G. S., Santee, W. R., & Erskine, D. J. (1985). Operative and standard operative temperature: Tools for thermal energetics studies. *American Zoologist*, *25*(4), 933–943. https://doi.org/10.1093/icb/25.4.933

Buckley, L. B., Ortiz, B. A. B., Caruso, I., John, A., Levy, O., Meyer, A. V., Riddell, E. A., Sakairi, Y., & Simonis, J. L. (2023). TrenchR: An R package for modular and accessible microclimate and biophysical ecology. *PLOS Climate*, *2*(8), e0000139. https://doi.org/10.1371/journal.pclm.0000139

Cox, C. L., Alexander, S., Casement, B., Chung, A. K., Curlis, J. D., Degon, Z., Dubois, M., Falvey, C., Graham, Z. A., Folfas, E., Koyner, M. A. G., Neel, L. K., Nicholson, D. J., Perez, D. J. P., Ortiz-Ross, X., Rosso, A. A., Taylor, Q., Thurman, T. J., Williams, C. E., … Logan, M. L. (2020). Ectoparasite extinction in simplified lizard assemblages during experimental island invasion. *Biology Letters*, *16*, 20200474. https://doi.org/10.1098/rsbl.2020.0474

Cox, C. L., Logan, M. L., Bryan, O., Kaur, D., Leung, E., McCormack, J., McGinn, J., Miller, L., Robinson, C., Salem, J., Scheid, J., Warzinski, T., & Chung, A. K. (2018). Do ring-necked snakes choose retreat

sites based upon thermal preferences? *Journal of Thermal Biology*, *71*, 232–236. https://doi.org/10.1016/j.jtherbio.2017.11.020

Cox, C. L., Tribble, H. O., Richardson, S., Chung, A. K., Curlis, J. D., & Logan, M. L. (2020). Thermal ecology and physiology of an elongate and semi-fossorial arthropod, the bark centipede. *Journal of Thermal Biology*, *94*, 102755. https://doi.org/10.1016/j.jtherbio.2020.102755

Davis, J., & Ford, R. G. (1983). Home range in the western fence lizard (*Sceloporus occidentalis occidentalis*). *Copeia*, *1983*, 933–940.

Deutsch, C. A., Tewksbury, J. J., Huey, R. B., Sheldon, K. S., Ghalambor, C. K., Haak, D. C., & Martin, P. R. (2008). Impacts of climate warming on terrestrial ectotherms across latitude. *Proceedings of the National Academy of Sciences of the United States of America*, *105*(18), 6668–6672. https://doi.org/10.1073/pnas.0709472105

Dzialowski, E. M. (2005). Use of operative temperature and standard operative temperature models in thermal biology. *Journal of Thermal Biology*, *30*(4), 317–334. https://doi.org/10.1016/j.jtherbio.2005.01.005

Faye, E., Rebaudo, F., Yánez-Cajo, D., Cauvy-Fraunié, S., & Dangles, O. (2016). A toolbox for studying thermal heterogeneity across spatial scales: From unmanned aerial vehicle imagery to landscape metrics. *Methods in Ecology and Evolution*, *7*(4), 437–446. https://doi.org/10.1111/2041-210X.12488

Fick, S. E., & Hijmans, R. J. (2017). WorldClim 2: New 1-km spatial resolution climate surfaces for global land areas. *International Journal of Climatology*, *37*(12), 4302–4315. https://doi.org/10.1002/joc.5086

Francis, R. J., Kingsford, R. T., & Brandis, K. J. (2022). Using drones and citizen science counts to track colonial waterbird breeding, an indicator for ecosystem health on the Chobe River, Botswana. *Global Ecology and Conservation*, *38*, e02231. https://doi.org/10.1016/j.gecco.2022.e02231

Garcia-Costoya, G. (2025). ggcostoya/throne-manuscript: throne-manuscript v.1.0. *Zenodo*. https://zenodo.org/records/15675999

Garcia-Costoya, G., Williams, C. E., Faske, T. M., Moorman, J. D., & Logan, M. L. (2023). Evolutionary constraints mediate extinction risk under climate change. *Ecology Letters*, *26*(4), 529–539. https://doi.org/10.1111/ele.14173

Gunderson, A. R., & Leal, M. (2012). Geographic variation in vulnerability to climate warming in a tropical Caribbean lizard. *Functional Ecology*, *26*(4), 783–793. https://doi.org/10.1111/j.1365-2435.2012.01987.x

Higgins, E. A., Boyd, D. S., Brown, T. W., Owen, S. C., van der Heijden, G. M. F., & Algar, A. C. (2024). Unoccupied aerial vehicles as a tool to map lizard operative temperature in tropical environments. *Remote Sensing in Ecology and Conservation*, *10*, 615–627. https://doi.org/10.1002/rse2.393

Hijmans, R. J. (2020). *terra: Spatial data analysis. R package Version 1.8–8*. CRAN.

Huey, R. B., Kearney, M. R., Krockenberger, A., Holtum, J. A. M., Jess, M., & Williams, S. E. (2012). Predicting organismal vulnerability to climate warming: Roles of behaviour, physiology and adaptation. *Philosophical Transactions of the Royal Society, B: Biological Sciences*, *367*(1596), 1665–1679. https://doi.org/10.1098/rstb.2012.0005

Jiao, L., Dong, D., Zhao, X., & Han, P. (2016). Compensation method for the influence of angle of view on animal temperature measurement using thermal imaging camera combined with depth image. *Journal of Thermal Biology*, *62*, 15–19.

Karger, D. N., Conrad, O., Böhner, J., Kawohl, T., Kreft, H., Soria-Auza, R. W., Zimmermann, N. E., Linder, H. P., & Kessler, M. (2017). Climatologies at high resolution for the earth's land surface areas. *Scientific Data*, *4*(1), 170122. https://doi.org/10.1038/sdata.2017.122

Kearney, M. R., & Porter, W. P. (2017). NicheMapR—An R package for biophysical modelling: The microclimate model. *Ecography*, *40*(5), 664–674. https://doi.org/10.1111/ecog.02360

Lemos-Espinal, J. A., Smith, G. R., & Ballinger, R. E. (2001). Sexual dimorphism and body temperatures of *Sceloporus siniferus* from Guerrero, México. *Western North American Naturalist*, *61*(4), 498–500.

Logan, M. L., Cox, R. M., & Calsbeek, R. (2014). Natural selection on thermal performance in a novel thermal environment. *Proceedings of the National Academy of Sciences of the United States of America*, *111*(39), 14165–14169. https://doi.org/10.1073/pnas.1404885111

Logan, M. L., Duryea, M. C., Molnar, O. R., Kessler, B. J., & Calsbeek, R. (2016). Spatial variation in climate mediates gene flow across an Island archipelago. *Evolution*, *70*(10), 2395–2403. https://doi.org/10.1111/evo.13031

Logan, M. L., Fernandez, S. G., & Calsbeek, R. (2015). Abiotic constraints on the activity of tropical lizards. *Functional Ecology*, *29*(5), 694–700. https://doi.org/10.1111/1365-2435.12379

Logan, M. L., Huynh, R. K., Precious, R. A., & Calsbeek, R. G. (2013). The impact of climate change measured at relevant spatial scales: New hope for tropical lizards. *Global Change Biology*, *19*(10), 3093–3102. https://doi.org/10.1111/gcb.12253

Logan, M. L., Neel, L. K., Nicholson, D. J., Stokes, A. J., Miller, C. L., Chung, A. K., Curlis, J. D., Keegan, K. M., Rosso, A. A., Maayan, I., Folfas, E., Williams, C. E., Casement, B., Gallegos Koyner, M. A., Padilla Perez, D. J., Falvey, C. H., Alexander, S. M., Charles, K. L., Graham, Z. A., … Cox, C. L. (2021). Sex-specific microhabitat use is associated with sex-biased thermal physiology in Anolis lizards. *Journal of Experimental Biology*, *224*(2), jeb235697. https://doi.org/10.1242/jeb.235697

Maclean, I. M. D., Mosedale, J. R., & Bennie, J. J. (2019). Microclima: An r package for modelling meso- and microclimate. *Methods in Ecology and Evolution*, *10*(2), 280–290. https://doi.org/10.1111/2041-210X.13093

Meyer, A. V., Sakairi, Y., Kearney, M. R., & Buckley, L. B. (2023). A guide and tools for selecting and accessing microclimate data for mechanistic niche modeling. *Ecosphere*, *14*(4), e4506. https://doi.org/10.1002/ecs2.4506

Neel, L. K., Logan, M. L., Nicholson, D. J., Miller, C., Chung, A. K., Maayan, I., Degon, Z., DuBois, M., Curlis, J. D., Taylor, Q., Keegan, K. M., McMillan, W. O., Losos, J. B., & Cox, C. L. (2021). *Habitat structure mediates vulnerability to climate change through its effects on thermoregulatory behavior*. https://doi.org/10.1098/rstb.2016.0146

Nicholson, D. J., Knell, R. J., McCrea, R. S., Neel, L. K., Curlis, J. D., Williams, C. E., Chung, A. K., McMillan, W. O., Garner, T. W. J., Cox, C. L., & Logan, M. L. (2022). Climate anomalies and competition reduce establishment success during island colonization. *Ecology and Evolution*, *12*(10), e9402. https://doi.org/10.1002/ece3.9402

Plasman, M., Gonzalez-Voyer, A., Bautista, A., & Díaz de la Vega-Pérez, A. H. (2024). Flexibility in thermal requirements: A comparative analysis of the wide-spread lizard genus *Sceloporus*. *Integrative Zoology*, 1–17.

Playà-Montmany, N., & Tattersall, G. J. (2021). Spot size, distance and emissivity errors in field applications of infrared thermography. *Methods in Ecology and Evolution*, *12*(5), 828–840. https://doi.org/10.1111/2041-210X.13563

Potter, K., Davidowitz, G., & Woods, H. A. (2009). Insect eggs protected from high temperatures by limited homeothermy of plant leaves. *Journal of Experimental Biology*, *212*(21), 3448–3454.

R Core Team. (2024). *R: A language and environment for statistical computing*. R Foundation for Statistical Computing.

Saunders, D., Nguyen, H., Cowen, S., Magrath, M., Marsh, K., Bell, S., & Bobruk, J. (2022). Radio-tracking wildlife with drones: A viewshed analysis quantifying survey coverage across diverse landscapes. *Wildlife Research*, *49*(1), 1–10. https://doi.org/10.1071/WR21033

Sears, M. W., & Angilletta, M. J. (2015). Costs and benefits of thermoregulation revisited: Both the heterogeneity and spatial structure of temperature drive energetic costs. *The American Naturalist*, *185*(4), E94–E102. https://doi.org/10.1086/680008

Sears, M. W., Angilletta, M. J., Schuler, M. S., Borchert, J., Dilliplane, K. F., Stegman, M., Rusch, T. W., & Mitchell, W. A. (2016). Configuration of the thermal landscape determines thermoregulatory performance of ectotherms. *Proceedings of the National Academy of Sciences of the United States of America*, *113*(38), 10595–10600. https://doi.org/10.1073/pnas.1604824113

Sheldahl, L. A., & Martins, E. P. (2000). The territorial behavior of the western fence lizard, *Sceloporus occidentalis*. *Herpetologica*, *56*, 469–479.

Sinervo, B., Méndez-de-la-Cruz, F., Miles, D. B., Heulin, B., Bastiaans, E., Villagrán-Santa Cruz, M., Lara-Resendiz, R., Martínez-Méndez, N., Calderón-Espinosa, M. L., Meza-Lázaro, R. N., Gadsden, H., Avila, L. J., Morando, M., De la Riva, I. J., Sepulveda, P. V., Rocha, C. F. D., Ibargüengoytía, N., Puntriano, C. A., Massot, M., … Sites, J. W. (2010). Erosion of lizard diversity by climate change and altered thermal niches. *Science*, *328*(5980), 894–899. https://doi.org/10.1126/science.1184695

Thiele, S. T., Varley, N., & James, M. R. (2017). Thermal photogrammetric imaging: A new technique for monitoring dome eruptions. *Journal of Volcanology and Geothermal Research*, *337*, 140–145. https://doi.org/10.1016/j.jvolgeores.2017.03.022

Thomas, C. D., Cameron, A., Green, R. E., Bakkenes, M., Beaumont, L. J., Collingham, Y. C., Erasmus, B. F. N., de Siqueira, M. F., Grainger, A., Hannah, L., Hughes, L., Huntley, B., van Jaarsveld, A. S., Midgley, G. F., Miles, L., Ortega-Huerta, M. A., Peterson, A. T., Phillips, O. L., & Williams, S. E. (2004). Extinction risk from climate change. *Nature*, *427*(6970), 145–148. https://doi.org/10.1038/nature02121

Webster, C., Westoby, M., Rutter, N., & Jonas, T. (2018). Three-dimensional thermal characterization of forest canopies using UAV photogrammetry. *Remote Sensing of Environment*, *209*, 835–847. https://doi.org/10.1016/j.rse.2017.09.033

Williams, C., Kueneman, J., Nicholson, D., Rosso, A., Folfas, E., Casement, B., Gallegos-Koyner, M., Neel, L., Curlis, J. D., McMillan, W., Cox, C., & Logan, M. (2022). Sustained drought, but not short-term warming, alters the gut microbiomes of wild Anolis lizards. *Applied and Environmental Microbiology*, *88*, e00530-22. https://doi.org/10.1128/aem.00530-22

Woods, H. A., Dillon, M. E., & Pincebourde, S. (2015). The roles of microclimatic diversity and of behavior in mediating the responses of ectotherms to climate change. *Journal of Thermal Biology*, *54*, 86–97. https://doi.org/10.1016/j.jtherbio.2014.10.002

Yuan, W., & Hua, W. A. (2022). A case study of vignetting nonuniformity in UAV-based uncooled thermal cameras. *Drones*, *6*(12), 394. https://doi.org/10.3390/drones6120394

SUPPORTING INFORMATION

Additional supporting information can be found online in the Supporting Information section at the end of this article.

Figure S1. Our study site in the Great Basin Desert, NV, USA (GPS 39.868 N, 119.627 W).

Figure S2. Western fence lizard (*Sceloporus occidentalis*) on the left and OTM on the right.

Figure S3. Fluctuation in operative temperature over the validation 1 period.

Figure S4. Correlation between operative temperatures and surface temperatures before applying corrections (left panel), after correcting for GCPs (middle panel), and after correcting for GCPs and the `correct_flights_data` function of the `throne` package (right panel) for validation 1 (top) and validation 2 (bottom).

Figure S5. Temperature bias observed for validation 1 (A) and validation 2 (B) expressed as a difference between operative and drone surface temperatures as a function of time of day.

Figure S6. Temperature bias observed for validation 1 is expressed as a difference between operative and drone surface temperatures as a function of day of the year.

Figure S7. Predicted thermal landscape generated for our study site in Northern Nevada generated for four Julian dates at five time points of the day.

Figure S8. Daily frequency distribution of error (predicted-observed temperature) across different combinations of `knot_p` parameters, numbers of OTMs and drone flights for validation 1.

Figure S9. Daily frequency distribution of error (predicted-observed temperature) across different combinations of `knot_p` parameters, numbers of OTMs and drone flights for validation 2.

Figure S10. Daytime only frequency distribution of error (predicted-observed temperature) across different combinations `knot_p` parameters, numbers of OTMs and drone flights for validation 1.

Figure S11. Daytime only frequency distribution of error (predicted-observed temperature) across different combinations `knot_p` parameters, numbers of OTMs and drone flights for validation 1.

Figure S12. Prediction error as a function of time of day across different combinations of `knot_p` parameters, numbers of OTMs and drone flights for validation 1.

Figure S13. Matching error between tiles and the OTMs that best describe them for validation 2.

Figure S14. Example of a cubic spline (orange) fitted to OTM measurements (black) that logged every 2 min across 24 h using 1, 2, 4 and 30 knots/h.

Figure S15. Results of processing the same flight at a spatial resolution of 0.5, 1 and 4 m^2.

Table S1. List of microhabitats where OTMs were deployed with corresponding descriptions and numbers of OTMs deployed (*N*) for validation 1 and 2.

Table S2. Flight metadata for validation 1 and 2.

Table S3. Mean predictive error (±SD) for validation 2, presented as the relative difference between the observed (from OTMs) and predicted (from the final thermal landscape output by throne) temperatures across different combinations of number of drone flights, number of OTMs, and knot_p values (magnitude of smoothing of raw OTM data; knots per hours are given in the brackets) used to generate the final thermal landscape.

Table S4. Mean predictive error (±SD) for validation 1 and 2, presented as the absolute difference between the observed (from OTMs) and predicted (from the final thermal landscape output by throne) temperatures across different combinations of number of drone flights, number of OTMs, and knot_p values (magnitude of smoothing of raw OTM data; knots per hours are given in the brackets) used to generate the final thermal landscape.

Table S5. Mean predictive error (±SD) for validation 1 and 2, presented as the relative difference between the observed (from OTMs) and predicted (from the final thermal landscape output by `throne`) temperatures across different combinations of number of drone flights, number of OTMs, and `knot_p` values (magnitude of smoothing of raw OTM data; knots per hours are given in the brackets) used to generate the final thermal landscape.

Appendix S1. Methodology for Validation 2.

How to cite this article: Alujević, K., Garcia-Costoya, G., Ratia, N., Schmitz, E., Godkin, R. S., Gopal, A. C., Bujan, J., & Logan, M. L. (2025). Using aerial thermography to map terrestrial thermal environments in unprecedented detail. *Methods in Ecology and Evolution*, *16*, 1688–1702. https://doi.org/10.1111/2041-210X.70096